



Title	Ion-temperature-gradient-driven transport in a density modification experiment on the tokamak fusion test reactor
Author(s)	Horton, W. ; Lindberg, D. ; Kim, J. Y. et al.
Citation	Physics of Fluids B. 1992, 4(4), p. 953-966
Version Type	VoR
URL	https://hdl.handle.net/11094/78520
rights	This article may be downloaded for personal use only. Any other use requires prior permission of the author and AIP Publishing. This article appeared in Physics of Fluids B: Plasma Physics 4, 953 (1992) and may be found at https://doi.org/10.1063/1.860112 .
Note	

The University of Osaka Institutional Knowledge Archive : OUKA

<https://ir.library.osaka-u.ac.jp/>

The University of Osaka

Ion-temperature-gradient-driven transport in a density modification experiment on the Tokamak Fusion Test Reactor

Cite as: Physics of Fluids B: Plasma Physics **4**, 953 (1992); <https://doi.org/10.1063/1.860112>

Submitted: 30 September 1991 . Accepted: 15 January 1991 . Published Online: 04 June 1998

W. Horton, D. Lindberg, J. Y. Kim, J. Q. Dong, G. W. Hammett, S. D. Scott, M. C. Zarnstorff, and S. Hamaguchi



View Online



Export Citation

ARTICLES YOU MAY BE INTERESTED IN

[Electron temperature gradient driven turbulence](#)

Physics of Plasmas **7**, 1904 (2000); <https://doi.org/10.1063/1.874014>

[Comparisons and physics basis of tokamak transport models and turbulence simulations](#)

Physics of Plasmas **7**, 969 (2000); <https://doi.org/10.1063/1.873896>

[Ion temperature-gradient-driven modes and anomalous ion transport in tokamaks](#)

Physics of Fluids B: Plasma Physics **1**, 1018 (1989); <https://doi.org/10.1063/1.859023>



Ion-temperature-gradient-driven transport in a density modification experiment on the Tokamak Fusion Test Reactor

W. Horton, D. Lindberg, J. Y. Kim, and J. Q. Dong

Institute for Fusion Studies, The University of Texas at Austin, Austin, Texas 78712

G. W. Hammett, S. D. Scott, and M. C. Zarnstorff

Princeton Plasma Physics Laboratory, P.O. Box 451, Princeton, New Jersey 08544

S. Hamaguchi

IBM Research Division, Thomas J. Watson Research Center, Yorktown Heights, New York 10598

(Received 30 September 1991; accepted 15 January 1992)

Tokamak Fusion Test Reactor (TFTR) profiles from a supershot density-modification experiment [Zarnstorff *et al.*, *Plasma Physics and Controlled Nuclear Fusion Research*, 1990, Proceedings of the 12th International Conference, Washington (IAEA, Vienna, 1991), Vol. I, p. 109] are analyzed for their local and ballooning stability to toroidal η_i modes in order to understand the initially puzzling results showing no increase in χ_i when a pellet is used to produce an abrupt and large increase in the η_i parameter. The local stability analysis assumes that $k_{\parallel} = 1/qR$ and ignores the effects of shear, but makes no assumption on the magnitude of $k_{\parallel} v_{ti}/\omega$. The ballooning stability analysis determines a self-consistent linear spectrum of k_{\parallel} 's including the effect of shear and toroidicity, but it expands in $k_{\parallel} v_{ti}/\omega \leq 1$, which is a marginal assumption for this experiment. Nevertheless, the two approaches agree well and show that the mixing length estimate of the transport rate does not change appreciably during the density modification and has a value close to or less than the observed χ_i , in contrast to most previous theories, which predicted χ_i 's that were over an order-of-magnitude too large. However, still to be explained is the observed increase of $\chi_i(r)$ with minor radius by adding the effects of (i) the finite-beta drift wave—magnetohydrodynamic (MHD) mode coupling, (ii) the slablike mode, or (iii) the trapped-electron response. The experimental tracking $0.2 < \chi_e/\chi_i < 0.7$ suggests that both grad T_i and trapped-electron driving mechanisms are operating.

I. INTRODUCTION

Transport studies in the large tokamak confinement devices show that the ion and electron thermal transport rates are well above the collisional neoclassical transport rates. When the thermal losses are expressed in terms of thermal diffusivities χ_i and χ_e , the lost rates are characterized as having comparable diffusivities $\chi_i \sim \chi_e$ with the order-of-magnitude of χ consistent with the $\mathbf{E} \times \mathbf{B}$ transport diffusion expected from small-scale drift wave turbulence. Drift wave stability theory predicts that typical tokamak discharges are unstable to drift waves driven by both the ion and the electron temperature and density gradients. An important stability parameter controlling the onset and the strength of the turbulence is the ratio of the density gradient scale length L_n to the temperature gradient scale length L_T called the eta parameter $\eta = L_n/L_T$.

Early pellet fueling experiments in the Alcator-C tokamak¹ showed the onset of improved confinement with the steepening of the density profile which is readily interpreted in terms of the ion temperature gradient drift wave turbulence due to the simultaneous sharp decrease in the η_i stability parameter. Similarly, improved confinement regimes in numerous other machines have been interpreted in terms of steepening the density gradient so as to lower the η_i and η_e stability parameters. In such an example, the ASDEX team² used density profile control to extend the unsaturated Alca-

tor energy confinement scaling $\tau_E \propto \bar{n}_e$ by a factor of 2 above the original saturation limit.

These various transport results show the need for a detailed study of the ion thermal transport in terms of drift wave turbulence theory. A series of transport studies on the Tokamak Fusion Test Reactor (TFTR) were undertaken by Scott *et al.*^{3,4} and Zarnstorff *et al.*^{5,6} to test the hypothesis that the ion transport is due to the ion-temperature-gradient-driven drift wave turbulence.

Earlier comparisons of TFTR experimental results with the existing ion temperature gradient (ITG) theories yielded mixed results. A set of measurements³ in the hot-ion and supershot regimes showed that theories gave χ_i 's that were 10–100 times too big in the plasma core ($r < a/3$). However, these theories were derived in the $\eta_i \gg \eta_{\text{crit}}$ limit and did not contain a smooth transition to zero transport as η_i dropped below η_{crit} where the ITG mode becomes stable. It was observed that these plasmas were actually close to marginal stability (see Fig. 2 of Ref. 3), which would explain the differences between the measured and theoretical χ_i . In fact, the correlation of the measured η_i with the theoretical η_{crit} (see Fig. 4 of Ref. 3) suggested that the plasma was forced to stay near marginal stability by the strong ITG transport, which would result if $\eta_i \gg \eta_{\text{crit}}$. A later set of experiments,⁴ which included L-mode plasmas found that some plasmas were able to have $\eta_i \gg \eta_{\text{crit}}$, but these tended to be colder plasmas for which the theoretical χ_i was perhaps not strong

enough to enforce marginal stability.

These findings lead to the experiments by Zarnstorff *et al.*,^{5,6} where the density profile of a hot supershot plasma was modified by a deuterium pellet or by helium gas injection to flatten the density profile and force $\eta_i \gg \eta_{crit}$. It was expected that a very large χ_i would then be observed in the experiment, but, in fact, χ_i changed very little, thus disproving the idea that marginal stability was enforced and calling into question the existing ITG theories. The focus of the work presented here is to analyze one of the discharges from this series in detail to try to understand this puzzling result.

We focus on TFTR discharge No. 44669 which is described in Table I and Fig. 1. This discharge was a “super-shot” plasma with $\tau_E \approx 2.7\tau_E^L$ and was heated by 14 MW balanced neutral beam injection in a 1 MA, 4.8 T target plasma with major radius $R = 2.45$ m and minor radius $a = 0.80$ m. A deuterium pellet was injected at $t = 4.50$ sec and penetrated only part way into the plasma, transiently producing a flat density profile corresponding to very large values of the stability parameters η_i and $\epsilon_n = L_n/R$. In the figures and tables, the letters A and B are used to designate the plasma state before and after the pellet injection. Figure 2 shows the radial profile of $\chi_i(r)$ obtained from the ion power balance analysis. As shown in Fig. 3, L_{T_i} did not change much (in fact, it dropped slightly), but because of the large rise in L_n , the stability limit for L_{T_i} was greatly exceeded for a period of more than 20 msec, much longer than the growth time for ITG instabilities. There was little change in the thermal diffusivities inferred from the power balance during these transients in TFTR, in apparent contrast to the earlier experiments in Alcator-C and ASDEX, and in disagreement with the existing theories that predicted very large values of χ_i if $\eta_i \gg \eta_{crit}$.

To illustrate the magnitude of the disagreement between theory and experiment, Fig. 2 compares the measured $\chi_i(r)$ before and after the pellet perturbation with several different theories: the analytic toroidal formula of Biglari *et al.*⁷ (BDR), and the numerically derived slab formula of Hamaguchi and Horton.⁸ [We have replaced the factor $(1 + \eta_i)$ that appeared in the original analytic formulas with the factor $(\eta_i - \eta_{crit})$, a modification motivated by the desire to

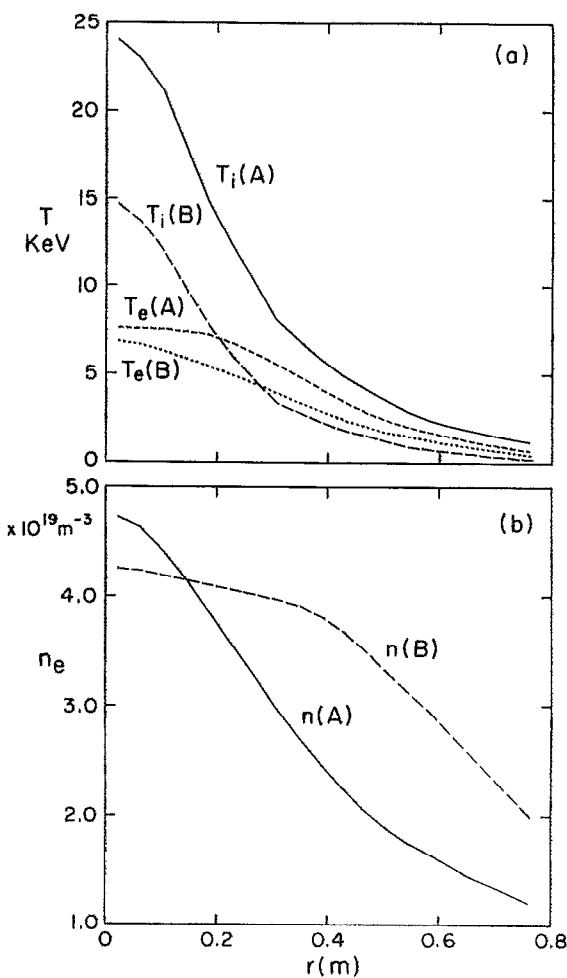


FIG. 1. Profiles of temperature and density for discharge 44669 in the A and B states.

have a reasonable transition to marginal stability and by the form of the Hamaguchi and Horton numerically derived χ_i .] These previous theories predict χ_i 's that are 1–2 orders of magnitude too large in the core of the plasma.

Developing a complete first-principles theory of tokamak turbulence is not a realistic task in the foreseeable future because of a multitude of active processes in the tokamak plasmas.⁹ The standard picture of tokamak turbulence is based on drift-wave-type instabilities (including the η_i mode and trapped electron modes) that generate small-scale $\mathbf{E} \times \mathbf{B}$ convective turbulence (although there is some uncertainty, both theoretically and experimentally, about whether small or large scale lengths dominate the transport). In order to make analytic progress and derive simple expressions for χ_i and χ_e , various approximations are made about the geometry (slab or toroidal), the dominant driving force (such as η_i), the mode structure, the collisionality, the nonlinear saturation mechanisms, and the nonlinear spectrum. The most complete formulas for χ_i to date are based on parametrization of three-dimensional (3-D) nonlinear computer simulations using a two-component hydrodynamic description of the plasma.

The ITG theories shown in Fig. 2 were based on a num-

TABLE I. TFTR perturbative transport discharges: shot number 44669, TRANSP number 2200, $r = 0.3$ m.

Time into discharge	4.490 sec	4.525 sec
$n_e (\times 10^{19} \text{ m}^{-3})$	3.03	3.98
T_e (keV)	5.71	4.07
T_i (keV)	8.4	3.55
L_n/R	0.17	1.18
L_{T_i}/R	0.074	0.056
η_i	2.3	21
T_e/T_i	0.68	1.15
α_{MHD}	0.36	0.29
\tilde{s}	0.75	0.7
q	1.52	1.53

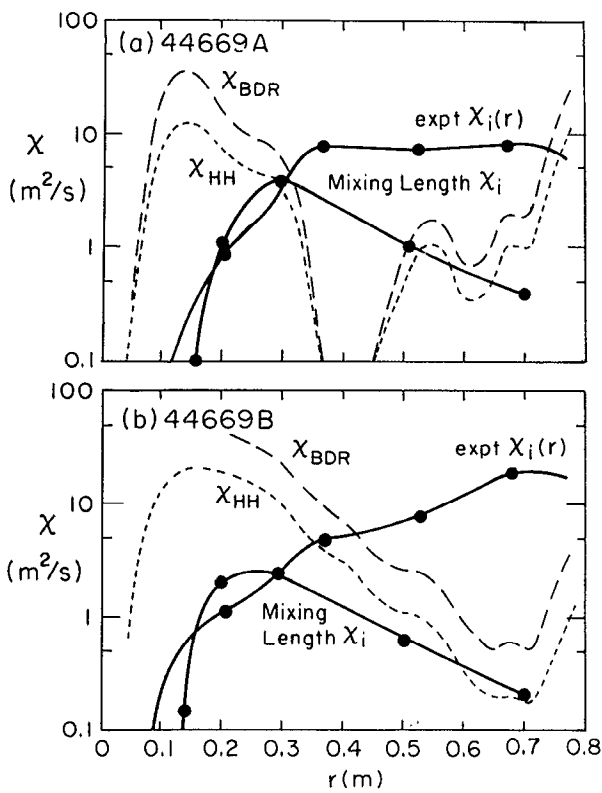


FIG. 2. Comparison of three theoretical models of ion thermal conductivity with experimental results for shot 44669 A and B states.

ber of simplifications, which caused them to predict a χ_i that is clearly too large. These theories were based on simplified fluid equations that did not adequately model finite-gyroradius effects or kinetic effects such as Landau damping (there is ongoing work to improve the fluid equations in this regard¹⁰ and to use more complex fluid models¹¹). More accurate kinetic (particle) simulations¹² show that the actual growth rates and mode widths should be significantly smaller than given by the simplified fluid equations. Fortu-

nately, both fluid and kinetic simulations seem to support the mixing length theory and the scaling law analysis for the turbulent diffusivities based on the characteristics of the most unstable linear modes. Table II gives the ion and electron diffusivities estimated from earlier theoretical works.

In this work, we show that a simple mixing length estimate applied to local kinetic theory, which incorporates toroidal and finite-gyroradius effects (missing from the previous theories) into a simple mixing length model is actually fairly consistent with the measured χ_i in the core of the plasma ($r < a/3$). However, the ITG mode appears to be too weak to explain the observed transport in the region $r > a/3$, where either some other mode must be invoked or the simple mixing length estimate fails.

Some of the observed radial profile of $\chi_i(r)$ is obtained in the inner region when we use the local kinetic theory that retains the full particle-wave resonance effects from the magnetic curvature and ∇B drift and the parallel ion transit drift. The local kinetic analysis¹³ shows that the threshold for the ion-temperature-gradient-driven turbulence η_{crit} is a function of $q(r)$. The q value determines the connection length $q(r)R$ between the good and bad toroidal curvature regions as well as the ratio of the strength of the ion Landau resonance from $k_{||}v_{||}$ to the grad- B curvature drift resonance $\omega_D = k_y v_D (v_{||}^2, v_{||}^2)$. Both these effects work together to make the η_i threshold higher at low q . Using this aspect of kinetic theory in the turbulence formulas for χ_i produces an increase of $\chi_i(r)$ with radius in the core region.

The present η_i theories seem to be insufficient to explain the radial dependence of χ_i in the outer region. Here, we consider the possibilities of obtaining the observed increase of χ_i with r/a by adding the effects of (i) the finite-beta drift wave magnetohydrodynamic (MHD) mode coupling, (ii) the slablike mode, or (iii) the trapped electron resonance, all of which are found to be inadequate. We also discuss other possible effects such as small-scale oscillations in the gradients or an unmeasured $\mathbf{E} \times \mathbf{B}$ poloidal shear flow as possible mechanisms for increasing the mixing width ΔX of the η_i modes in the outer region.

The structure of the paper is as follows. In Sec. II, the

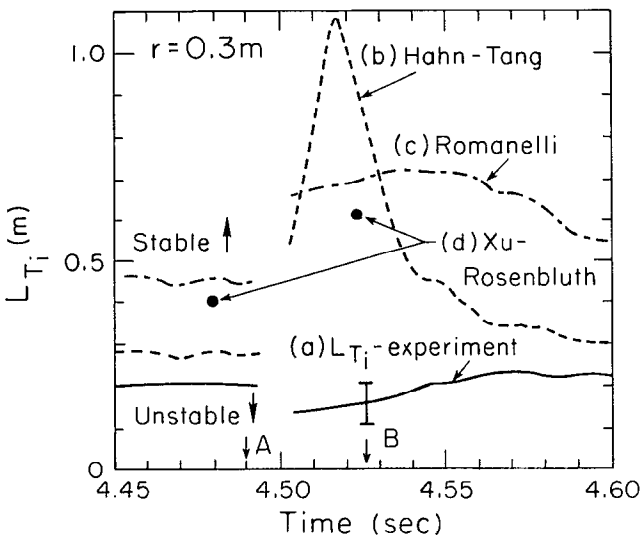


FIG. 3. Comparison of three theoretical models of critical temperature gradient length (L_T) with experimental result at $r = 0.3$ m as a function of time. The reference times for states A and B are marked.

TABLE II. TFTR drift wave turbulent diffusivities: shot 44669 at $r = 0.3$ m.

	$t_A = 4.490$	$t_B = 4.525$
χ_i^{exp}	$= 4 \text{ m}^2/\text{sec}$	$3 \text{ m}^2/\text{sec}$
D_{dw}	$= (\rho_s/a)(cT_e/eB)$	
$\chi_e^{(1)}$	$= 3.45 \text{ m}^2/\text{sec}$	$2.07 \text{ m}^2/\text{sec}$
	$= av_e c^2 / qR^2 \omega_{pe}^2$	
$\chi_e^{(2)}$	$= 2.58 \text{ m}^2/\text{sec}$	$1.66 \text{ m}^2/\text{sec}$
	$= (a/R)^{1/2} (\rho_s c T_e / a e B)$	
χ_i^{HH}	$= 1.97 \text{ m}^2/\text{sec}$	$3.85 \text{ m}^2/\text{sec}$
	$= (\rho_s c T_i / L_n e B) (\eta_i - \eta_{ic})$	$\frac{\rho_s c T_i}{L_T e B} \exp\left(-4 \frac{T_e L_T}{T_i L_s}\right)$
	$\times \exp(-5\hat{s}) = 9.1 \text{ m}^2/\text{sec}$	$= 12 \text{ m}^2/\text{sec}$
χ_i^{BDR}	$= (q/\hat{s}) \omega_{*e} \rho_i^2 (1 + \eta_i)$	
	$= 8.1 \text{ m}^2/\text{sec}$	$5.0 \text{ m}^2/\text{sec}$
$\chi_{i,Local-Vlasov}^{KH}$	$= \gamma_m / k_m^2$	
	$= 5.2 \text{ m}^2/\text{sec}$	$2.4 \text{ m}^2/\text{sec}$

transport in TFTR discharge 44669 is compared with various models of the η_i mode. First, a detailed analysis is given from the local kinetic theory. Then the electrostatic and electromagnetic ballooning analysis is followed to complement the local analysis. Also, the sheared slab model is discussed for completeness. In Sec. III, in the attempts to solve the disagreement problem of the radial profile of χ_i at the outer region, various stability effects such as steeper edge gradients and trapped electron resonance are discussed. Finally, in Sec. IV, the conclusions are summarized.

II. DRIFT WAVE STABILITY ANALYSIS

A. Local electrostatic kinetic analysis

We begin the analysis of the discharge by determining the unstable spectrum from local, electrostatic stability theo-

ry using the parameters from Table I. For Maxwellian velocity distributions, the electrostatic dispersion relation is

$$D_{ES}(k, \omega) = \sum_j \frac{n_j e_j^2}{T_j} \left(1 - \left\langle \frac{\omega - \omega_{*j}(\epsilon)}{\omega - \omega_{Dj} - k_{\parallel} v_{\parallel}} J_0^2 \right\rangle \right). \quad (1)$$

The j summation is over electrons, ions, and impurities. In Sec. III B, we briefly consider the effect of the carbon impurities on the stability. When only the thermal ions are taken as dynamical with the electrons and beam ions as adiabatic, the dispersion relation (1), in the standard dimensionless units, reduced to

$$D_{ITG}(k_y, k_{\parallel}, \omega) = D_a - \int_0^{\infty} \int_{-\infty}^{+\infty} \frac{\{\tau\omega - k_y [1 + \eta(v^2/2 - 3/2)]\} J_0^2(k_{\perp} v_{\perp} / \tau^{1/2}) e^{-v^2/2} v_{\perp} dv_{\perp} dv_{\parallel}}{\tau\omega - k_y \epsilon_n (\frac{1}{2} v_{\perp}^2 + v_{\parallel}^2) - k_{\parallel} v_{\parallel} \tau^{1/2}} \frac{v_{\perp} dv_{\perp} dv_{\parallel}}{(2\pi)^{1/2}}, \quad (2)$$

where the adiabatic response D_a is given by

$$D_a = 1 + \frac{n_i T_e}{n_e T_i} + \frac{n_b T_e}{n_e T_b} + \frac{n_z Z^2 T_e}{n_e T_z} [1 - I_0(b_z) e^{-b_z}]. \quad (3)$$

In Eq. (3), we include a hydrodynamic impurity ion contribution where $b_z = k_{\perp}^2 \rho_z^2$, and we assume the impurity drift frequency $\omega_{*z} = 0$. The adiabatic response reduces to the usual $D_a \approx 1 + T_e/T_i$ of ideal ITG mode theory when the impurity and beam densities are sufficiently low. The usual dimensionless parameters in Eq. (2) are $\epsilon_n = r_n/R$ with $r_n = L_n = -(\partial \ln n / \partial r)^{-1}$, and $\tau = T_e/T_i$ and the fluctuation variables k_{\perp} , k_{\parallel} , and ω are normalized to $\rho_s = c_s/\omega_{ci}$, r_n , and r_n/c_s with $c_s = (T_e/m_i)^{1/2}$.

The marginal stability analysis of the dispersion relation in (2) gives the condition $\eta_i > 2/3$ and

$$\epsilon_T = \epsilon_n / \eta < 0.7 / D_a \quad (4)$$

for the threshold of instability. The toroidal threshold condition (4) is derived by Dominguez and Waltz¹⁴ and Horton *et al.*¹⁵ and is often called the Romanelli¹⁶ condition

$$\left(\frac{L_{T_i}}{R} \right)_{\text{crit}} = \frac{0.7}{1 + T_i/T_e}, \quad (5)$$

since Romanelli emphasized its practical importance. Clearly, the role of magnetic shear is considered subdominant when applying conditions (4) or (5) since the formulas are independent of s .

In the case where the magnetic shear length $L_s(r)$ is relatively short ($L_s < R$), the results of marginal stability from the sheared-slab eigenmode analyses in the flat density profile limit are given by Hahm and Tang¹⁷

$$\left(\frac{L_{T_i}}{L_s} \right)_{\text{crit}}^{-1} = \frac{3}{2} \sqrt{\frac{\pi}{2}} \left(1 + \frac{T_i}{T_e} \right) (2l + 1). \quad (6)$$

Here, $l = 0, 1, 2, \dots$ is the radial mode number.

Both stability conclusions (5) and (6) state that, for fixed scale lengths, the system is stable when T_e/T_i falls below a critical value $(T_e/T_i)_{\text{crit}}$. In both the A and B states, we find that the plasma is well above this critical value τ_{crit} , as shown in Fig. 3. As a function of $\tau = T_e/T_i$, the growth rate first increases as $\tau - \tau_{\text{crit}}$ and then decreases as $(1/\tau)^{1/2}$ for $\tau \gg \tau_{\text{crit}}$. In the hydrodynamic approximation, Hamaguchi and Horton⁸ give

$$\gamma_k \approx |\omega_{*e}| \left[\left(\frac{\eta_i S}{2\tau} \right)^{1/2} - \frac{S}{2} \left(1 + \frac{3}{4} \frac{\Gamma}{\tau} \right) \right] \quad (7)$$

with η_{crit} in the flat density limit given by $\eta_{\text{crit}} = (ST_e/2T_i) [1 + \frac{3}{4}(\Gamma/\tau)]^2$, where Γ is the ideal gas constant and $S = L_n/L_s$. The maximum $\gamma_k(\tau)$ occurs at $\tau_m = \Gamma^2 S / \eta$ with the value of $\gamma_m = \frac{1}{2} |\omega_{*e}| (\eta_i/\Gamma - \frac{3}{4} S)$. The local stability analysis indicates that the experiment is in the regime of γ_k decreasing with increasing τ . The comparison of the stability conditions on L_{T_i} for the transport discharge is given in Fig. 3 showing that the plasma is unstable to both criteria at all times. The critical values for L_{T_i} obtained by the integral equation analysis by Xu and Rosenbluth¹⁸ are also shown to be close to the value from the Romanelli formula given by the curve labeled (c).

While the threshold formulas given in Eqs. (4)–(7) are useful, a simpler and more direct picture of the stability of the system is obtained by finding all the local eigenmodes $\omega_k(r)$, $\gamma_k(r)$ from the Vlasov dispersion relation. The sheared slab and ballooning modes may be viewed as certain linear superpositions of these local modes that form long-lived states in the inhomogeneous system. We calculate such local solutions both varying the radial position and the poloidal angle to obtain a description of the stability of the system before and after the pellet injection.

In Fig. 4, we show the spectrum of $\gamma(k_y, k_{\parallel}, r)$ computed from Eq. (2) (with $n_b = n_z = 0$) before (state A) and during the flat density profile perturbation (state B).

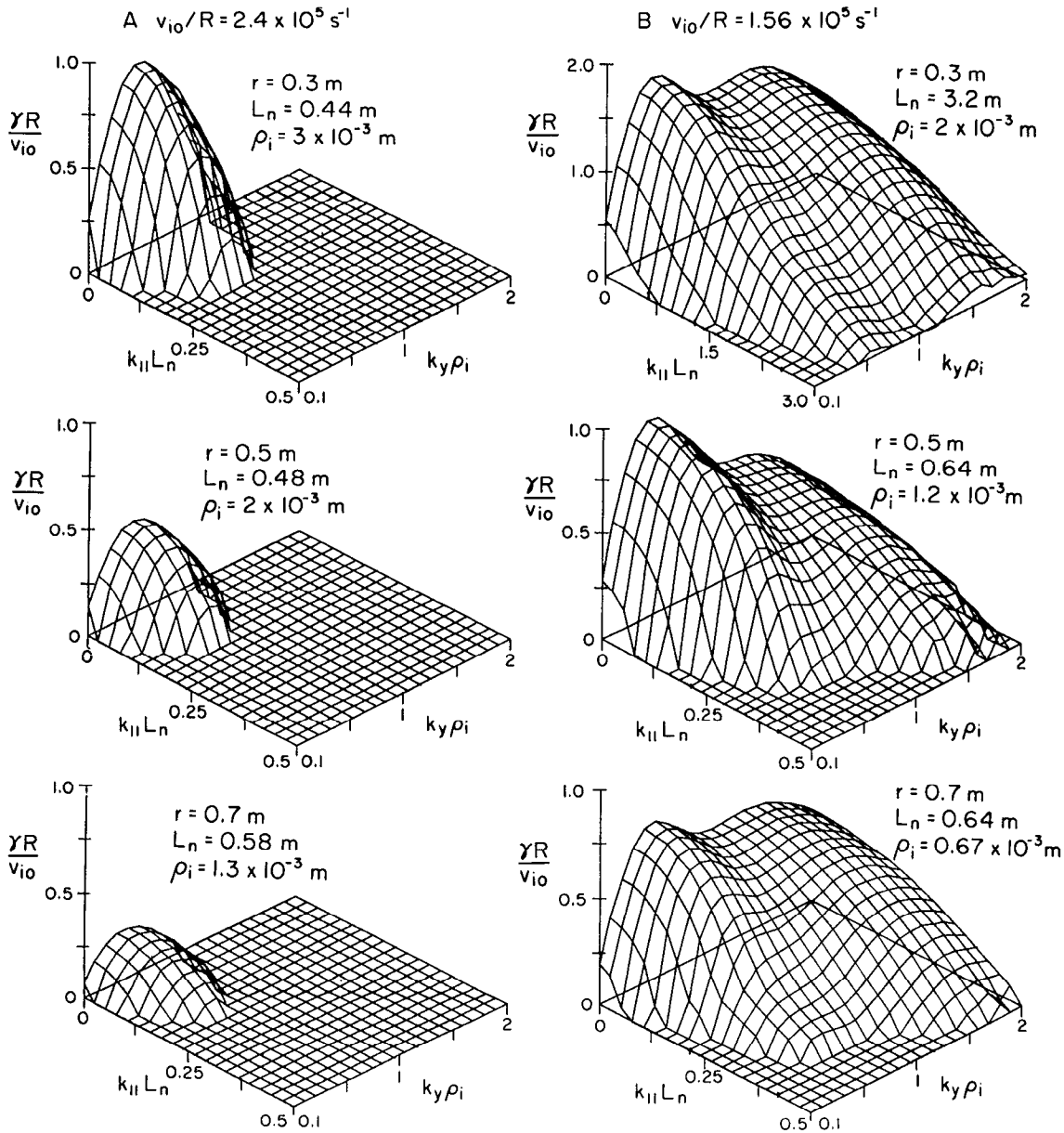


FIG. 4. The local kinetic growth rates in the wave-number domain for the shot 44669 A and B states.

The growth rates in Fig. 4 are normalized by v_{io}/R ($2.4 \times 10^5 \text{ sec}^{-1}$) for state A and v'_{io}/R ($1.56 \times 10^5 \text{ sec}^{-1}$) for state B, where v_{io} and v'_{io} are the ion thermal velocity $(T_i/m_i)^{1/2}$ at $r = 0.3 \text{ m}$ in the states A and B, respectively. We see that, in both states, there is a large spectrum of unstable wave numbers. The principal effect of the large increase in η_i is to destabilize the modes with $k_{||} \rho_i > 1$. In fact, in the flat profile state, a secondary local maximum is produced at $k_{||} \rho_i \sim 1.5$, which is a stable region before the density flattening. However, these short-wavelength modes may not have a significant effect on the transport because nonlinear 3-D simulation studies^{8,12} support the theoretical picture that the correct measure of the transport is $\gamma/k_x^2 \sim \gamma/k_y^2$, since the turbulent states are found to

be isotropic $\langle k_x^2 \rangle \sim \langle k_y^2 \rangle$ with the peak of the k_y spectrum only slightly down shifted from the k_x , which maximizes γ_{k_y} depending on η_i , ϵ_n , and s . The secondary instability giving rise to the isotropization in $k_x - k_y$ is analyzed in Cowley *et al.*¹⁹

The long-wavelength modes ($k_{||} \rho_i < 1$) have the maximum dimensionless growth rate $\gamma_m L_n / c_s$ increasing with the increase of η_i . However, during the perturbation, the value of L_n and the ion temperature T_i change strongly (see Fig. 1). Thus, returning to the actual growth rate, we find that, at $r = 0.3 \text{ m}$, the maximum growth rate γ_m is slightly increased from $2.1 \times 10^5 \text{ sec}$ to $2.6 \times 10^5 \text{ sec}$ and its location shifts from $k_m = 2 \text{ cm}^{-1}$ to $k_m = 3.2 \text{ cm}^{-1}$. Fluid turbulence simulations imply that the expected turbulent trans-

port is then $\chi_i(r = 0.3 \text{ m, A}) = \gamma_m/k_m^2 = 5.2 \text{ m}^2/\text{sec}$ compared with $\chi_i(r = 0.3 \text{ m, B}) = 2.4 \text{ m}^2/\text{sec}$. While numerous parameters change from the A to B states of the discharge, the dominant change for the χ_i value at $r = 0.3 \text{ m}$ is the decrease of the ion temperature from 8.4 to 3.55 keV. In Table III, the mixing length values of χ_i , obtained from the local Vlasov stability analysis described by Eq. (1), are given at various radii for the A and B states.

From the local analysis, we also see that the degree to which the local parameters are in the toroidal regime of small $k_{\parallel} v_T/\omega_{Di}$ in contrast to the sheared slab regime with $x = k_{\parallel} v_T/\omega_{Di} > 1$ is an important influence on the stability of the ITG modes. As analyzed in detail in Kim and Horton¹³ and Dominguez and Rosenbluth,²⁰ this dependence on $k_{\parallel} v_T/\omega_{Di} \sim 1/qk_y\rho$ taking $k_{\parallel} = 1/qR$ gives a q dependence to the growth rate $\gamma_{\max}(q)$, the threshold η_{crit} , and the associated transport. In Fig. 2, we plot the results given in Table III labeled as "mixing length χ_i ," and compare with experimental results. The kinetic mixing length $\chi(r)$ in Fig. 2 has a radial dependence that is in considerably better agreement with the experimental profile at the inner region of $r < a/3$ than the $\chi_i^{\text{HH}}(r)$ and $\chi_i^{\text{BDR}}(r)$ formulas. However, at the outer region of $r > a/2$, there is still significant disagreement in the radial dependence. The unfavorable radial dependence arises from the rapid decrease of $T_i(r)$, which overcomes the increase of χ_i with q at fixed T_i .

B. Electrostatic ballooning mode stability analysis

Here, we analyze the stability of the system to the electrostatic ballooning mode equation assuming that the ion acoustic dynamics $k_{\parallel}^2 c_s^2/\omega^2$ can be expanded to first order in the kinetic response functions in Eq. (1). The ballooning eigenmode equation gives the proper averaging over the spectrum of parallel wavelengths that occurs at each $k_y\rho_s$ and radius. The change in the eigenvalues from the local value given in Sec. II A occurs from the ion acoustic wave propagation along the magnetic field lines. Many basic studies of the drift wave ballooning mode equation for the η_i mode problem from numerous groups are available as reviewed in Horton.⁹ Here, we give the ballooning mode equation used in the study with minimal explanation for the present application. The electrostatic mode equation²¹ is

$$\left[\left(1 - \frac{\omega_{*i}}{\omega} \right) \Gamma_0 - \frac{\omega_{*i}}{\omega} \eta_i [\Gamma_0 + b(\Gamma_1 - \Gamma_0)] \right] \frac{\epsilon_n^2}{q^2 \omega^2} \frac{\partial^2 \phi}{\partial \theta^2} + \{1 + \tau[1 - P(\theta)]\} \phi(\theta) = 0 \quad (8)$$

with the boundary conditions $\phi(\theta \rightarrow \infty) \rightarrow 0$ sufficiently rap-

TABLE III. Mixing length χ_i from local Vlasov theory: shot 44669, using γ_{\max} at $k_{\parallel} = 1/qR$, and $\langle k_x^2 \rangle = \langle k_y^2 \rangle = k_y^2(\gamma_{\max})$.

r	Before injection	After injection
0.15 m	0.0 m ² /sec	0.16 m ² /sec
0.3 m	5.2 m ² /sec	2.4 m ² /sec
0.5 m	1.2 m ² /sec	0.7 m ² /sec
0.7 m	0.4 m ² /sec	0.21 m ² /sec

idly for $\langle k_x^2 \rangle \propto s^2 k_y^2 \int_{-\infty}^{\infty} \theta^2 \phi^2 d\theta$ to exist. In Eq. (8), the kinetic response function P , given in Eq. (A3) in the Appendix, is a function of θ and vanishes as $1/\theta^2$ for large θ . The local perpendicular and parallel wave numbers are given by

$$k_{\perp}^2 \rho_i^2 = (k_y^2 \rho_s^2 / \tau) (1 + s^2 \theta^2),$$

$$k_{\parallel} = -\frac{i}{qR} \frac{1}{\phi} \frac{\partial \phi}{\partial \theta},$$

and the local grad- B and curvature drift frequency is

$$\omega_{Di} = -\epsilon_n k_y \rho_s \frac{m_i}{T_i} \left(\frac{1}{2} v_{\perp}^2 + v_{\parallel}^2 \right) (\cos \theta + s \theta \sin \theta) \left(\frac{c_s}{L_n} \right)$$

for low-beta, circular flux surfaces.

The ballooning mode equation (8) has a series of eigenfunctions describing the normal modes of the plasma. As in the sheared slab, we designate the l th mode by $\phi_{k_y l}(\theta)$ and order the modes with increasing oscillations with $l = 0, 1, 2, \dots$. Important measures of the characteristics of the modes are given by the integral width $\Delta\theta_i$ and the differential width $\Delta\theta_D$. We also define the mean value of the expansion parameter $P_{\parallel} = \overline{k_{\parallel}^2} v_i^2 / \omega^2$ used in obtaining the differential equation (8) from the integral mode equation. The definitions of the $\phi(\theta)$ measures are

$$\Delta\theta_i^2 = \frac{\int_0^{\infty} d\theta \theta^2 \phi^2(\theta)}{\int_0^{\infty} d\theta \phi^2(\theta)}, \quad (9)$$

$$\frac{1}{\Delta\theta_D^2} = \frac{\int_0^{\infty} d\theta [\phi'(\theta)]^2}{\int_0^{\infty} d\theta \phi^2(\theta)}. \quad (10)$$

The ballooning mode wave function $\phi(\theta)$ gives a ballooning mode radial width ΔX_b and k_x given by

$$\langle k_x^2 \rangle = \Delta X_b^{-2} = k_y^2 s^2 \text{Re}(\Delta\theta_i^2), \quad (11)$$

with the subscript b for ballooning. This ballooning mode width and the associated $\gamma/\langle k_x^2 \rangle$ has been estimated theoretically in Horton *et al.*²² and Dominguez and Rosenbluth.²⁰ The resulting diffusivities are similar to that given as χ^{BDR} in Table II. The ballooning χ_i varies inversely proportionally with shear $s = r q' / q$ and proportionally to q , which, for fixed T_i , gives a χ_i that increases with r/a .

The expansion parameter for measuring the strength of the ion acoustic wave effect is $\langle k_{\parallel}^2 \rangle v_i^2 / \omega^2$, which, in the dimensionless variables, is given by

$$P_{\parallel} = \frac{T_i}{T_e} \frac{\epsilon_n^2}{q^2} \frac{1}{|\omega|^2 |\Delta\theta_D^2|}, \quad (12)$$

and the validity of the differential Eq. (8) requires that $P_{\parallel} < 1$. Now, using Eq. (8), we consider the ballooning stability of the modes identified as most dangerous from the local stability analysis in Sec. II A.

For each radial position in Table III, we have carried out the integration of the ballooning mode equation in Eq. (8) to find the lowest-order eigenmodes and eigenvalues. First of all, the ballooning mode analysis shows that there are two important fast growing modes: One is peaked at $\theta = 0$, which we call the outside mode and one peaked in the region $\theta = \pi/3$ to $2\pi/3$, which we call the top/bottom mode since the peak intensity is somewhere in those regions rather than on the outside. The shapes of the eigenfunctions of these

modes are shown in Fig. 5 for $r = 0.3$ m before and after injection. Generally, the growth rates of the top/bottom modes are about one-half that of the outside mode and the frequency of the top/bottom mode is 1.5 times greater than the outside mode. Both frequencies are generally somewhat above the local kinetic transit frequency $k_{\parallel} v_i$ obtained with $k_{\parallel} = 1/qR$. We find that the growth rates of the outside mode are close to those obtained with the local kinetic theory.

We have computed the moments of the wave functions defined in Eqs. (9) and (10) to determine the expansion parameter P_{\parallel} and radial mode with ΔX_b . We find that, even though the condition $P_{\parallel} < 1$ is marginally satisfied over most radii, the outside mode growth rates are nearly equal to the local kinetic results. The top/bottom mode has a larger P_{\parallel} than the outside mode, and thus is closer to the slab mode. The mode widths ΔX_b 's appear to be larger than ρ_s over all radii before and after the discharge, so that the diffusivity estimate based on $\gamma \Delta X_b^2$ is somewhat larger than the isotropic turbulence mixing length $\Delta X_{ml} = k_y^{-1}$. For example, for 44669 A and $r = 0.3$ m, we obtain $\Delta X_b/\rho_s = 2.9$ with $P_{\parallel} = 0.20$ so that $\chi_i^b = 6.8$ m²/sec compared with 5.2 m²/sec from $\Delta X_{ml} = 1/k_y(\gamma_{\max})$. It must be emphasized that the mode width ΔX_b from Eq. (11) corresponds to the linear regime. From the nonlinear studies,^{8,9,12,19} however, we recognize that the nonlinear saturation forces the formation of approximately circular vortices so that the proper mixing length is k_y^{-1} when $k_y \Delta X_b > 1$. Now, with this consideration the results from the ballooning mode calculation using $\Delta X_{ml} = 1/k_y(\gamma_{\max})$ are given in Table IV. Comparing Table III and Table IV, we see that the ballooning mode analysis agrees quite well with the local kinetic analysis.

The expansion used to derive Eq. (8) is only valid if $P_{\parallel} \ll 1$, which is marginally satisfied for our parameters. Calculating moments of the eigenfunction and using Eqs. (10)

TABLE IV. Mixing length χ_i from electrostatic ballooning equation: shot 44669, using $\chi_i = \gamma_m \Delta X_{ml}^2$ and $\Delta X_{ml}^2 = k_y^{-2}(\gamma_m)$.

r	Before injection	After injection
0.15 m	0.19 m ² /sec	0.13 m ² /sec
0.3 m	5.1 m ² /sec	2.2 m ² /sec
0.5 m	1.23 m ² /sec	0.68 m ² /sec
0.7 m	0.37 m ² /sec	0.21 m ² /sec

and (12), we find that $P_{\parallel} = 0.2$ for the outside mode at $r = 0.3$ m at time A. Nevertheless, the growth rates for the outside mode from the ballooning equation, Eq. (8), are close ($\Delta\gamma/\gamma \lesssim 20\%$) to the growth rates found from the local dispersion relation, Eq. (2), which made no expansion in P_{\parallel} . This gives some confidence that this calculation is approximately correct, at least for the outside mode, which is primarily driven by toroidal curvature. The good comparison between the two approaches is due in part to the use of $k_{\parallel} = 1/qR$ in the local theory, which agrees well with average k_{\parallel} calculated by our ballooning equation. However, it is possible that a more complete ballooning calculation that does not depend on a small P_{\parallel} ordering might produce a different spectrum of k_{\parallel} 's. This may be important because part of the drop of the theoretical χ_i near the axis is due to the stabilization of the ITG mode at large k_{\parallel} because of the assumed k_{\parallel} dependence on $1/q$, which is getting large near the axis.

An interesting area for future work would be to apply a more complete ballooning mode calculation that does not rely on this small P_{\parallel} approximation. In fact, comparing Fig. 14 of Ref. 18 (which makes no assumptions about k_{\parallel} or P_{\parallel}) with Fig. 4 of Ref. 20 (which makes $P_{\parallel} \ll 1$ and $k_{\parallel} = 1/qR$ approximations), one finds that the stabilization of ITG modes at low q is overstated by the $k_{\parallel} = 1/qR$ approximation.

While our expansions may be marginally acceptable for the outside mode, they are not useful for the top/bottom mode for which we find $P_{\parallel} \approx 7$ and $k_{\parallel} \approx 4/qR$. The top/bottom mode is not affected much by the toroidal curvature drive. We will analyze this slablike mode with a theory that is valid for general P_{\parallel} in Sec. II D.

C. Electromagnetic ballooning analysis

To complete the stability analysis of the discharges, we consider the electromagnetic ballooning mode analysis. Here, again, there are many works giving the details of the theoretical analysis including, but not limited to the ones of Cheng,²³ Tang *et al.*,²⁴ Hong *et al.*,²¹ and Dominguez and Moore.²⁵

Using the $\psi(\theta)$ potential for A_{\parallel} such that $E_{\parallel} = -ik_{\parallel}(\phi - \psi)$, we obtain the electromagnetic mode equation

$$\left[\frac{\omega_A^2}{\omega^2} \frac{\partial}{\partial \theta} k_{\perp}^2 \frac{\partial}{\partial \theta} + \left(1 - \frac{\omega_{*e}}{\omega} \right) \left(1 - \frac{\omega_{De}}{\omega} \right) - \frac{(1 - \omega_{*e}/\omega)^2}{D_{ES}(\omega, k, \theta)} \right] \psi = 0 \quad (13)$$

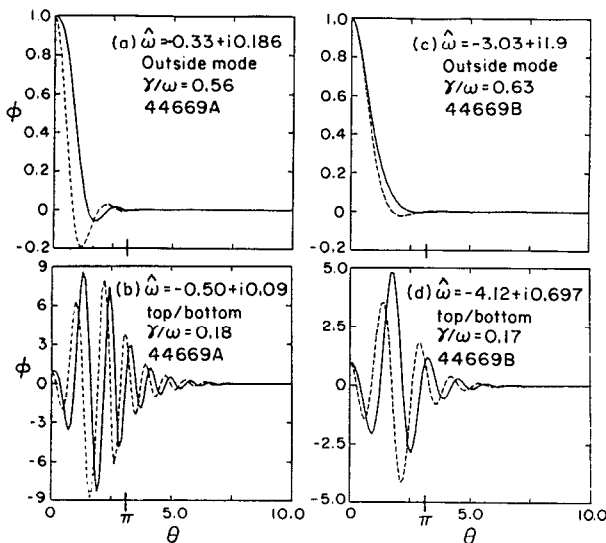


FIG. 5. The shapes of the kinetic ballooning eigenfunctions for both the outside and top/bottom modes at $r = 0.3$ m for 44669 A and B states.

valid for $P_{\parallel} < 1$. Some details of the derivation of Eq. (13) are given in the Appendix. The $s - \alpha$ equilibrium model is used as a simple approximation for the equilibrium. In this model, the local wave number and drift frequency become

$$k_{\perp}^2 = k_{y\rho_s}^2 [1 + (s\theta - \alpha \sin \theta)^2],$$

$$\omega_{Di} = \bar{\omega}_{Di} [\cos \theta + (s\theta - \alpha \sin \theta) \sin \theta], \quad (14)$$

giving the reversal of the magnetic shear for $\alpha > 1$. Here, $\alpha = -2Rq^2 d\beta/dr$, with β containing all the pressure components, and reaches a maximum value of 0.4 in 44669 A and B.

In Table V, we show the growth rates and real frequencies obtained from the local electromagnetic dispersion relation at various radii for the discharge 44669 before and during the density modification. The spectrum of modes obtained from Eq. (13) contains both the local electrostatic toroidal ITG mode, which has $\omega_A^2/\omega^2 \gg 1$ and thus satisfies Eq. (13) by having the electrostatic dispersion relation $D_{ES}(\omega, k, \theta) \approx 0$, and the high-frequency kinetic FLR-MHD mode rotating with

$$\omega \approx \omega_{*i} (1 + \eta_i).$$

The kinetic finite Larmor radius (FLR)-MHD mode is destabilized by the $\omega = \omega_{Di}$ drift resonance below the MHD beta limit α_{crit} .^{21,23,24} The α is sufficiently below α_{crit} in these discharges that kinetically modified FLR-MHD mode is a real oscillation with $\omega = -5.09 \times 10^6 \text{ sec}^{-1}$ at $r = 0.3 \text{ m}$ and $k_y \rho_s = 0.5$. Table V shows that the electromagnetic effect on the electrostatic toroidal ITG mode is stabilizing. For each radius, there are two modes with their polarization given in the right-hand column, where $E_{\parallel} = 0$ at $\psi/\phi = 1$ and $\delta B_r = 0$ at $\psi/\phi = 0$. On the other hand, to obtain the MHD ($k_y \rho \rightarrow 0$) beta limit, the mode equation (13) is expanded in the fluid limit to obtain

$$\frac{\epsilon_n^2}{q^2} \frac{2}{\beta_e} \frac{\partial}{\partial \theta} k_{\perp}^2 \frac{\partial}{\partial \theta} \psi + \left[\omega [\omega - \omega_{*i} (1 + \eta_i)] k_{\perp}^2 (\theta) + \omega_{*e} \omega_{De} (\theta) \left(1 + \eta_e + \frac{1 + \eta_i}{\tau} \right) \right] \psi = 0. \quad (15)$$

For 44669 A, Fig. 6(a) shows the shape of an eigenfunction of Eq. (15) for $r = 0.3 \text{ m}$, $k_y \rho_s = 0.5$ ($k_y = 2.2 \text{ cm}^{-1}$) before injection, where the eigenvalue is $\omega = -2.66 c_s/L_n$ ($3.13 \times 10^6 \text{ sec}^{-1}$) compared with $\omega_{*i} (1 + \eta_i) = -2.55 c_s/L_n$ ($3.01 \times 10^6 \text{ sec}^{-1}$) and $\omega_A = v_A/qR = 3.06 c_s/L_n$ ($3.6 \times 10^6 \text{ sec}^{-1}$) using $c_s/L_n = 1.18 \times 10^6/\text{sec}$. The ballooning mode width is $\Delta X_b = 0.342 \rho_s$. This compares well with kinetic modified (FLR)-MHD eigenmode given by Eq. (13) with $\omega = -2.87 c_s/L_n$ ($3.38 \times 10^6 \text{ sec}^{-1}$) and mode width $\Delta X_b = 0.342 \rho_s$ at the same position.

In Fig. 6(b) the η_i -mode branch of the same EM equation is found by solving Eq. (13) with the electrostatic eigenmode as the first-trial function. The electromagnetically modified η_i -mode solution has $\omega = (-0.277 + i0.0272) \times (c_s/L_n)$ or $(-32.7 + i3.21) \times 10^4 \text{ sec}^{-1}$ eigenvalue and the ballooning mode width $\Delta X_b = 0.690 \rho_s$. The electromagnetic modification has reduced γ and the estimated χ_i .

D. Electromagnetic integral equation analysis in sheared slab

In Secs. II A and II B, the ballooning mode analysis was made by expanding the parallel ion motion in the small $|k_{\parallel}^2 v_i^2/\omega^2|$ limit. Here, we study the slablike branch, called the top/bottom mode in Fig. 5, from another theoretical description taking into account $\omega \sim k_{\parallel} v_i$ for completeness. For the slablike mode, we use the integral equation code of Dong *et al.*²⁶ in the electromagnetic regime with nonadiabatic electrons. In the electrostatic limit with adiabatic electrons, the result gives the 44669 A maximum growth rate

TABLE V. Growth rates and real frequencies obtained from the dimensionless local electromagnetic dispersion relation at various radii for the discharge 44669.

r (m)	ω_A ($10^6/\text{sec}$)	ω ($10^5/\text{sec}$)	γ ($10^5/\text{sec}$)	k_{\parallel} (1/m)	k_{\perp} (1/cm)	ψ/ϕ	
Shot 44669 A							
0.30	3.58	— 3.51	1.64	0.268	2.18	— 0.104	0.0882
0.30	3.58	— 50.9	0	0.268	2.18	1.07	0
0.50	2.49	— 2.00	0.882	0.148	3.30	— 0.0746	0.0498
0.50	2.49	— 33.9	0	0.148	3.30	1.09	0
0.70	1.40	— 1.39	0.367	0.0699	5.14	— 0.105	0.0468
0.70	1.40	— 18.9	0	0.0699	5.14	1.08	0
Shot 44669 B							
0.30	3.11	— 3.93	2.55	0.267	2.57	— 0.0403	0.103
0.30	3.11	— 39.8	0	0.267	2.57	1.12	0
0.50	1.88	— 1.29	1.36	0.148	3.86	— 0.0259	0.0843
0.50	1.88	— 22.9	0	0.148	3.86	1.11	0
0.70	1.06	— 0.482	0.969	0.070	6.07	0.004 14	0.117
0.70	1.06	— 12.8	0	0.070	6.07	1.10	0

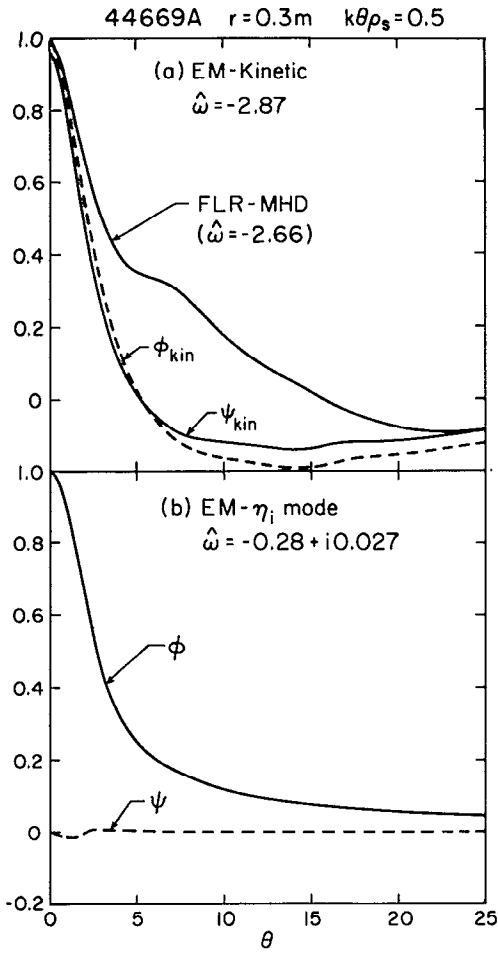


FIG. 6. The eigenfunctions of the electromagnetic kinetic and FLR-MHD ballooning modes. In (a), the stable kinetically modified FLR-MHD mode is given from Eq. (13) (kinetic) and Eq. (13) (FLR-MHD). In (b), the electrostaticlike mode from the electromagnetic equation (15) is given.

$\gamma_m = 9 \times 10^4/\text{sec}$ and the 44669 B value $\gamma_m = 6.5 \times 10^4/\text{sec}$ at $r = 0.15$ m.

Within the adiabatic approximation for the electron dynamics, the electromagnetic corrections are weak. However, the electromagnetic effects appear to be substantial at the inner radii when the assumption of adiabatic electron dynamics is released. For example, the integral equation analysis shows that, at $r = 0.15$ m, the electromagnetic-nonadiabatic electron systems have a growth rate of only $\gamma = 4 \times 10^3/\text{sec}$ for 44669 A and $\gamma = 4.1 \times 10^4/\text{sec}$ for 44669 B, which are notably smaller than the values given above for electrostatic limit with adiabatic electrons.

Because of the stabilizing effect of finite beta, some favorable radial dependence of $\chi_i(r)$ can be produced but the effect is found to be weak for discharge 44669.

The quasilinear heat flux taking into account the inductive electric field $\partial A_{\parallel}/\partial t$ and the perturbed magnetic field δB_{\perp} for both the ions and the electrons is given by

$$Q_j = -\frac{c^2 n_j T_j}{B^2} \sum_{\mathbf{k}} \int d^3 \mathbf{v} d\omega \left[\frac{1}{T_j} \frac{dT_j}{dx} \left(\frac{m_j v^2}{2T_j} - \frac{3}{2} \right) + \frac{1}{n_j} \frac{dn_j}{dx} - \frac{\omega e_j B}{ck_y T_j} \right] \left(\frac{mv^2}{2T_j} \right) \pi \delta(\omega - k_{\parallel} v_{\parallel})$$

$$\times k_y^2 J_0^2(k_{\perp} \rho) \left| \phi_{k\omega}(x) - \frac{v_{\parallel}}{c} A_{\parallel k\omega}(x) \right|^2. \quad (16)$$

Because of the slablike resonance approximation, this Q_j is proportional to $|E_{\parallel k\omega}(x)|^2/k_{\parallel}^2(x)$. For Q_i only, the large k_{\parallel} part of the wave number spectrum contributes and, for Q_e , only the small k_{\parallel} part of the spectrum contributes significantly. The solution of Ampère's law for A_{\parallel} shows that A_{\parallel} is not negligible compared with ϕ , so that the effective cross-field correlation length is increased by the finite beta coupling to A_{\parallel} . Using the electromagnetic quasilinear diffusion coefficients from Eq. (16) evaluated at the mixing length amplitude

$$(\Delta x)^2 = \left| \frac{\text{Re} \int x^2 [E_{\parallel}(x)]^2 dx}{\int [E_{\parallel}(x)]^2} \right|,$$

results in the electromagnetic diffusivity estimate of $\chi_i = \gamma(\Delta x)^2 = 0.77 \text{ m}^2/\text{sec}$ ($k_y \rho_s = 0.3$) compared with the electrostatic value of $\chi_i = 12 \text{ m}^2/\text{sec}$ ($k_y \rho_s = 0.5$) for 44669 A at $r = 0.15$ m. It is worth mentioning that $\chi_i = 2.45 \text{ m}^2/\text{sec}$ and $\chi_i = 0.30 \text{ m}^2/\text{sec}$ are obtained, respectively, from electrostatic and electromagnetic perturbations if $\chi_i = \gamma/k_y^2$ is used to estimate the diffusivity. The differences are sufficient to indicate that, for the slablike modes, the electrostatic approximation is breaking down in the plasma core.

III. OTHER STABILITY AND TRANSPORT EFFECTS

A. Effect of steeper edge gradients

The ion temperature T_i is only measured at a small set of discrete radial points, and it is conceivable that the $T_i(r)$ profile is not a simple smooth function but may have small-scale oscillations with some regions of large gradients dT/dr . In order to test the sensitivity of our theoretical χ 's to the experimentally measured gradients, "what if" numerical experiments are performed first of reducing L_{T_i} and then reducing both L_{T_i} and L_{n_i} by one-half at the radius $r = 0.7$ m. The results from local kinetic theory for 44669 A state are that the growth rates and χ_i increase to about two times the reference value for both the two gradient variations. Even these large changes in L_{T_i} and L_{n_i} seem to be insufficient to explain the experimental diffusivity result, which is over $10 \text{ m}^2/\text{sec}$ at $r = 0.7$ m.

B. Effect of carbon impurity

The dominant impurity is fully ionized ($Z = 6$) carbon. Since the gradient scale lengths for carbon are not well known, we first studied the effect of including the carbon component $\beta_c = n_c/n_e$ in Eq. (1) within the slab approximation with $\omega_*(C) = 0$. The growth rates are reduced to about one-half their $\beta_c = 0$ value when $\beta_c \simeq 0.1$ (or $Z^2 n_c/n_e \simeq 3.6$) in the A state and, in the B state, the effect is weaker with a reduction of about 2/3 in the growth rate. Taking $\omega_*(C) \simeq -\omega_*$ leads to stronger stabilization with

the A state becoming stable for $\beta_c \gtrsim 0.05$ and the stability of the B state is, again, less affected by the carbon component.

C. Comparison with the Swedish stability and transport analysis

The plasma theory group²⁷ at Chalmers University, Sweden has developed a model of the stability and transport for the ion temperature and collisionless trapped electron temperature gradient instability that is reported to produce agreement with the power balance thermal diffusivities in some JET and TEXTOR discharges.²⁸ Their theoretical model differs from that presented here in the following aspects. The model uses collisionless two-component hydrodynamic equations in which the toroidal drift frequency ω_D is taken as completely dominant over the $k_{\parallel} v_i$ resonance. The effect of magnetic shear is neglected as is the role of ion acoustic waves. The recent version²⁹ of their theory contains a continued-fraction approximation for the reactive part of the drift resonance $\omega = \omega_D$, which seems to provide a fairly good fit to the $k_{\parallel} = 0$ kinetic results, even though the dissipative part (due to collisionless phase mixing) is ignored. (Extension to include the dissipative part might be done with a variation of the work of Hammett and Perkins.) Their theoretical modeling assumes the modes to be localized to the outside ($\theta = 0$) of the torus and that the spectrum of k_{\parallel} is sufficiently small to be negligible compared with the toroidal drift ω_D effects. The key parameters are then L_n/R and L_T/R , as well as the trapped electron fraction f_i and $\tau = T_e/T_i$. In the Swedish model, the stability, determined by the roots of a fourth-order polynomial in ω , gives a trapped electron mode rotating in the electron diamagnetic direction, which is used to calculate χ_e and an η_i mode rotating in the ion direction, which is used to determine the χ_i . We have solved their polynomial dispersion relation for TFTR discharge (44669) and find that their growth rates for the mode rotating in the ion direction are somewhat smaller than those obtained in the kinetic analysis in Sec. III A. A typical comparison is that, in the A state at $r = 0.5$ m before injection, their equation gives the ion mode $\omega + i\gamma = -0.612 + 0.0537i$ and the electron mode $\omega + i\gamma = 0.224 + 0.106i$ compared with the local kinetic value $\omega + i\gamma = -0.274 + 0.148i$ in unit c_s/L_n , where the adiabatic electron model used in Eq. (2) gives only the ion mode.

The second major difference is in the formula used for the amplitude of the potential fluctuations by the Swedish group. They modify the mixing length level by including a factor of γ/ω , so that the quasilinear formula for χ_i is now proportional to

$$\gamma^3 / [(\omega - \frac{1}{2}\omega_D)^2 + \gamma^2] \langle k_x^2 \rangle.$$

This makes their χ formulas vanish at the rate γ^3 as $\gamma \rightarrow 0$ as it does from large compressibility when $L_n/R \gtrsim 1$ in the plasma core. In this way, the resulting χ_i develops a radial profile that is closer in shape to the power balance $\chi_i(r)$ than that reported here in Table III. Nordman *et al.*²⁷ support their choice of the modified mixing length formula by appealing to agreement with a simple two-dimensional toroidal mode coupling simulation, which has no magnetic shear or $\omega_{Di}(\theta)$

variation. Their results for χ_i would appear, however, to contradict both the theoretical and simulation results obtained by Hamaguchi and Horton,⁸ where the χ_i is shown to vary as $\eta_i - \eta_{i,crit}$ at small γ , which is no faster than γ^2 and is close to γ for the slab model. Of course, the problem of obtaining accurate theoretical formulas for the saturation level is an unsolved problem, which leaves room for various models. For the near marginal states $\gamma \rightarrow 0$, bifurcation analysis⁸ gives a systematic calculation of the variation $\chi_i = (\eta_i - \eta_{i,crit})\chi_1$, which does not agree with the γ^3 variation in Nordman *et al.*²⁷ For comparison, we have applied the χ formulas of Nordman *et al.*²⁷ to the TFTR discharge. We find that their extra power of γ/ω in the fluctuation level formula and the $s = 0$ approximation have the effect of making the $\chi_i(r)$ increase with radius. The formulas have the problem, however, of predicting that $\chi_e \gg 4\chi_i$, contrary to theoretical expectations and to the power balance diffusivities that have^{3,4} $\chi_i > \chi_e$. For $\gamma_k \gg (\omega_k - \frac{1}{2}\omega_D)^2$, the Nordman *et al.*²⁷ χ_i formula reduces to the usual estimate of γ_k/k^2 , consistent with Hamaguchi and Horton away from marginal stability.

Rewoldt and Tang³⁰ find a different behavior for the effect of the trapped electron mode. They find one eigenmode with a Gaussian-like $\phi_{k_\theta}(\theta)$ that changes direction of rotation from the ion diamagnetic to electron diamagnetic as η_i is decreased below 1 to 1.5. They call this continuous root the hybrid mode. When the mode rotates in the electron direction, the growth rate has an enhancement due to the trapped electron contribution. For larger η_i , the growth is determined by the ion dynamics with $\gamma \simeq 1.25(1 + \eta_i) \times 10^4$ sec for $k_\theta \rho_s = 0.356$, $r/a = 0.21$ in the beam-heated TFTR discharge 22014. Their quasilinear transport studies show $\chi_i > \chi_e$ with χ_i and χ_e comparable to those obtained from power balance at the mixing length level.

One may conclude from these comparisons of theory with experiment, as is also obvious from the proportionality of the quasilinear thermal flux with the square of the amplitude, that the actual fluctuation levels increase more strongly toward the outside than given by the mixing length level formula as presently understood and applied. The problem of the disagreement in the radial profile of χ_i may be removed if actual measured fluctuation levels are used in the quasilinear formulas. A recent study by Bravenec *et al.*³¹ reports $\chi_e(r)$ using the measured fluctuation levels in the quasilinear formula in a study of electron power balance in TEXT. The study, however, still shows disagreement in the radial profile of $\chi_e(r)$ in the outer edge region of the Ohmic TEXT experiment. In all tokamaks, in both the L- and H-confinement modes, the measured fluctuation levels are, to the authors' knowledge, strongly increasing toward the plasma edge. The problem with the radial profiles $\chi_i(r)$ and $\chi_e(r)$ then appears to reduce to the fact that the mixing length fluctuation levels $\Delta X/L_T$ and $\Delta X/L_n$, given by theoretical formulas used to obtain χ_i , do not increase rapidly enough with radius. Perhaps, it is necessary to find more directly the mixing scales in the edge turbulence and to consider the long-correlated $\mathbf{E} \times \mathbf{B}$ drift orbits that occur in regions where the vortex rotation parameter⁹ $R_E = k_{\perp} \tilde{v}_E / \Delta \omega > 1$.

D. Trapped electron destabilization

When the profiles are such that the ion-temperature-gradient-driven turbulence is weak, it is necessary to calculate χ_i taking into the resonant trapped electron response as a drive to the same electrostatic drift modes $D_{ES}(k, \omega) = 0$. In classical η_i -mode theory, the resonant electron response is neglected since the contribution is subdominant for large η_i and of a different physical origin.

Because of the fast electron transit v_e/qR and bounce $\epsilon^{1/2}v_e/qR$ frequencies (with $\epsilon = r/R$) compared with the fluctuation frequencies, the electron response \tilde{n}_e is a bounce average of $\phi(\theta)$ over the parallel electron motion $\dot{\theta} = v_{\parallel}/qR = \pm [2(E - \mu B)]^{1/2}/qR$. For $B \simeq B_0(1 - \epsilon \cos \theta)$ and the pitch angle variable $\lambda = \mu B_0/E$, the argument of the elliptic function integrals $K(m)$ and $E(m)$ is given by

$$m_{\lambda} = \kappa^2 = \frac{1}{2} \left(1 + \frac{1 - \lambda}{\epsilon} \right) = \begin{cases} 0 & \text{at } \lambda = 1 + \epsilon \text{ (deeply trapped),} \\ 1 & \text{at } \lambda = 1 - \epsilon \text{ (separatrix).} \end{cases} \quad (17)$$

The pitch angle averaged trapped electron resonance is

$$H_e^{\text{Tr}}(k, \omega, w) = \int_{1-\epsilon}^{1+\epsilon} \frac{d\lambda}{\pi} \times \frac{\tau(m_{\lambda})}{\omega - \epsilon n_{\omega} w G(m_{\lambda}, s) + i\nu_{\text{eff}}/w^{3/2}}, \quad (18)$$

with the reduced quarter-bounce period $\tau(m_{\lambda}) = K(m_{\lambda}) \times (2/\lambda\epsilon)^{1/2}$, and

$$G(m_{\lambda}, s) = \left(-1 + \frac{2E(m_{\lambda})}{K(m_{\lambda})} \right) + 2s \left(\frac{2E(m_{\lambda})}{K(m_{\lambda})} - 2 + 2m_{\lambda} \right).$$

The trapped electron density response function is then

$$\tilde{n}_e = (n_e e \Phi / T_e) (1 - P_e^{\text{Tr}}) \quad (19)$$

with

$$P_e^{\text{Tr}} = \frac{2}{\pi^{1/2}} \int_0^{\infty} dw w^{1/2} e^{-w} \left\{ \omega - k_y \left[1 + \eta_e \left(w - \frac{3}{2} \right) \right] \right\} H_e^{\text{Tr}}(k, \omega, w). \quad (20)$$

The classical theory³² of the trapped electron mode follows from $D_{ES}^{\text{Tr}} = 1 - P_e^{\text{Tr}} + \tau [1 - P_i^{\text{Tr}}(\omega, k)] = 0$, where the nonresonant or hydrodynamic ion response function $P_i^{\text{Tr}}(\omega, k)$ is taken for the ions and the resonant electron response $\text{Im } P_e^{\text{Tr}}$ drives the turbulence through $\gamma_k = \text{Im } P_e^{\text{Tr}} / (\partial D_{ES} / \partial \omega)$. The nonadiabatic electron response in Eq. (19) gives a phase shift between \tilde{n}_e and $\tilde{\Phi}$ leading to particle transport.

For 44669 A at $r = 0.3$ m with $\eta_e = 1.22$, we find two roots of the electrostatic dispersion relation with P_e^{Tr} . The root with the largest γ has the behavior shown in Fig. 1 of Rewoldt and Tang³⁰ when η_i is varied from -5 to $+3$. For $\eta_i \gtrsim 2$ the growth rate is dominated by the η_i driving mechanism. The second root has a considerably smaller growth rate with $\gamma_2/\gamma_1 \lesssim 1/6$.

The trapped-electron driven turbulence produces $\mathbf{E} \times \mathbf{B}$ turbulent diffusion of the ions and electrons given in the quasilinear approximation by

$$\begin{aligned} \left(\frac{\Gamma}{q_e} \right) &= \frac{n_e c T_e}{e B} \sum_{\mathbf{k}\omega} \left| \frac{e \Phi_{\mathbf{k}}}{T_e} \right|^2 \frac{2}{\pi^{1/2}} \int_0^{\infty} dw w^{1/2} e^{-w} \\ &\times \left(\frac{1}{w - 3/2} \right) \left\{ \omega - k_y \left[1 + \eta_e \left(w - \frac{3}{2} \right) \right] \right\} \\ &\times \text{Im } G_e^{\text{Tr}}(\mathbf{k}, \omega, w), \end{aligned} \quad (21)$$

with the thermal fluxes Q_i and Q_e given by

$$Q_i = \frac{3}{2} T_i \Gamma_i + q_i \quad (22)$$

and

$$Q_e = \frac{3}{2} T_e \Gamma_e + q_e, \quad (23)$$

where the q_i and q_e are the conductive part of the thermal flux due to (the out-of-phase) \tilde{T}_j fluctuations. At the mixing length level of turbulence, where

$$(\tilde{n}_k / \bar{n}_e)^2 \simeq 1 / \langle k_x^2 L_n^2 \rangle \simeq (\rho_s^2 / L_n^2) (L_s / L_n),$$

these fluxes from the trapped electrons can explain the magnitude and some of the parametric variations found in tokamaks.^{31,33,34} In Bravenec *et al.*,³¹ the fluctuation spectrum measured by FIR scattering and the heavy ion-beam probe are used in the quasilinear formulas (21)–(23). The principal difficulty with using the trapped electron mode for χ_e in all regimes is the lack of a sufficiently strong q dependence and the tendency for the $q_e(r)$ flux to decrease rapidly with increasing radius r/a just as is the problem discussed above for the η_i -driven χ_i formulas.

A second source of electron thermal flux is obtained by including the short-wavelength ∇T_e -driven electromagnetic turbulence. This small-scale η_e -driven turbulence, which is the electron analog of the η_i , produces a collisionless skin depth electromagnetic χ_e given by trapped electrons

$$\chi_e = \epsilon^{1/2} \omega_{be} c^2 / \omega_{pe}^2 = r v_e c^2 / q R^2 \omega_{pe}^2. \quad (24)$$

As shown in Table II, rate $\chi_e^{(1)}$ from Eq. (24) can exceed that from the longer-wavelength part of the spectrum $\chi_e^{(2)}$. For fixed T_e , the electromagnetic χ_e in Eq. (24) vanishes with electron mass $m_e \rightarrow 0$ as $m_e^{1/2}$, whereas the electrostatic χ_e in Eq. (21) is independent of m_e , which indicates the physically different origins of these transport components. The relationship between the $\chi_e^{(1)}$ skin depth transport and the $\chi_e^{(2)}$ trapped electron mode is analyzed in Kim *et al.*³⁵

IV. CONCLUSION

The TFTR supershot density-modification experiment of Zarnstorff *et al.*^{5,6} has been analyzed for local and ballooning mode stability to the η_i modes. The analysis shows that, even though the ion temperature gradient parameter η_i increases almost an order of magnitude ($\eta_i = 2.3 \rightarrow 21$ at $r = 0.3$ m) from the flattening of the density profile, the growth rate and wave number of the dominant η_i modes are not strongly changed. The ion thermal diffusivity constructed from the linear kinetic growth rate and the isotropic turbulent correlation length $\Delta X_{\text{ml}} \sim k_m^{-1}$ as required by the 3-D turbulence simulations, yields a decrease in χ_i in the post

injection state due to (1) the lowering of the ion and electron temperatures and (2) the increase of the toroidicity parameter ϵ_n to the order of unity where compressibility is strongly stabilizing. The toroidal η_i -mode growth rate $\gamma_k(\epsilon_n, \eta_i)$ has a maximum at small ϵ_n for fixed η_i .

The stability analysis from both the local and nonlocal equations shows that the discharges are not near marginal stability. Even within the classical η_i -mode approximation of adiabatic electrons, the ∇T_i -driven modes are unstable both before and after pellet injection. The ion thermal diffusivities derived here are not sufficiently large to force the profiles to marginal stability.

The previous theories predicted χ_i 's that were much larger than observed in the experiment. Our present calculations do a better job by including a number of important effects that were not adequately treated in previous theories. Finite-gyroradius and kinetic effects (such as Landau damping) are retained, which reduce the growth rate significantly, which is partially offset by the inclusion of toroidal driving terms that had been missing from many of the previous theories that were in slab geometry. Also, we use a shorter mixing length $1/|k_y|$ rather than a longer mixing length, which sometimes is suggested by the linear radial mode structure but which is not expected to survive the nonlinear regime.

There are a number of ways in which future work could build upon our calculations. We have employed local toroidal calculations that are good for arbitrary $k_{\parallel} v_{ti}/\omega$ but which assume a $k_{\parallel} = 1/(qR)$, and we have used a ballooning mode equation expanded for small $k_{\parallel} v_{ti}/\omega$ but which self-consistently determines a linear spectrum of k_{\parallel} 's. Although we have found good agreement between the two approaches, it would be interesting to repeat the stability analysis using more complicated ballooning codes that do not assume small $k_{\parallel} v_{ti}/\omega$. We have used a simple s - α model equilibrium, but a more accurate equilibrium would, among other things, introduce a nonlocal dependence on integral quantities through the Shafranov shift $\Delta(r)$. At the edge of this plasma ($r \geq 0.65$ m), $\Delta' = -(a/R)(\beta_p + l_i/2) = -0.65$ is large, giving an enhancement in the pressure gradient by a factor of 2 to 3 while also shortening the connection length by a similar factor.

The present η_i mode theories fail, however, to explain the radial dependence of the power balance χ_i over all radii, in particular, at the outer edge region. Attempts to obtain the observed increase of $\chi_i(r)$ with r/a by adding the effects of (i) the finite-beta drift wave-MHD mode coupling, (ii) the slablike mode, or (iii) the trapped electron resonances are found to be inadequate. The tracking $0.2 \leq \chi_e/\chi_i \leq 0.7$ suggests that both the ∇T_i and the collisionless-trapped-electron driving mechanisms are operating. The disagreement in the χ_i and χ_e profiles appear to arise from the underestimate by theory of the actual fluctuation levels that are measured to increase strongly with radius.

The problem of the lack of agreement in the radial variation of the theoretical turbulent conductivities compared with the experimental power balance conductivities occurs for many forms of microturbulence. The conflict suggests one of several possibilities: (i) that another class of linear

instabilities is controlling transport in the outer regions, (ii) that either the relevant gradient scale lengths $L_n(r)$, $L_T(r)$ in the dynamics of the plasma are substantially shorter in the region $r/a > 0.5$ than reported from the measured mean (temporally and spatially smoothed) profiles $n_j(r)$, $T_j(r)$, or (iii) that the actual mixing length ΔX_{ml} is substantially greater than the theoretical values. Indeed, there is evidence on a number of tokamaks that the theories underestimate the actual fluctuation levels that are measured to increase strongly with radius. Theoretical transport effects outside the scope of the usual locally homogeneous turbulence models related to the radial profiles of the gradient parameters, the shear profile, and the $\mathbf{E} \times \mathbf{B}$ shear flows created in the outer layer of the plasma may be responsible for the larger edge transport. The effect of a strongly localized $\mathbf{E} \times \mathbf{B}$ shear flow layer³⁶⁻³⁸ can distort the radial wave functions, and thus increase the radial mixing length. Studies of the shear flow layer effect are advancing and show that, if the shear flow scale length L_E for the nonuniform flow $v_E(r)$ satisfies $v'_E = v_E/L_E > (c_s/L_s)$, the Kelvin-Helmholtz-like vortices are formed between the counter-flowing plasma streams. In this shear flow layer, the mixing width ΔX_{ml} becomes as large as the vortex diameter, which is found to approach L_E for sufficiently small L_E .³⁸

Other mechanisms for increasing the mixing length may be the electromagnetic shielding of the induced parallel current filaments by the collisionless skin depth c/ω_{pe} , which exceeds $\rho_s (L_s/L_n)^{1/2}$ at sufficiently low β_e characteristic of the edge region,^{9,35} and long-correlated $\mathbf{E} \times \mathbf{B}$ orbits in the amplitude regime above the mixing length level.³⁹

In this work, we have clarified the basic problems that occur in using present theoretical models for understanding and analyzing power balance in the supershot regime in the TFTR.

ACKNOWLEDGMENTS

The authors thank Professor D. E. Baldwin for his encouragement and critical comments on the project during his tenure as Director of the Institute for Fusion Studies. We thank P. C. Efthimion, G. Schmidt, and the rest of the TFTR team at the Princeton Plasma Physics Laboratory (PPPL) who (along with M. C. Zarnstorff) performed the original experiments and provided us with access to the data.

The work was supported by U.S. Department of Energy Contract No. DE-FG05-80ET-53088 and PPPL Contract No. DE-AC02-76-CHO-3073.

APPENDIX: ELECTROMAGNETIC BALLOONING MODE EQUATIONS

The calculations of the Vlasov parallel current and charge densities are given in Cheng,²³ Hong *et al.*,²¹ and Horton *et al.*⁴⁰ The ballooning mode representation of the fields in a torus is used, and the mode frequencies are taken to be between the transit frequencies of the ions and electrons which is justified *a posteriori*. The condition of quasineutrality is

$$\hat{a}\phi + \hat{b}\psi = 0 \quad (\text{A1})$$

and the parallel component of Ampère's law is

$$\hat{b}\phi + \hat{d}\psi = 0, \quad (\text{A2})$$

where

$$\hat{a}(k, \omega, \theta) = -1 + \tau(P-1) - \frac{c_s^2}{\omega^2 q^2 R^2} \frac{\partial}{\partial \theta} P_3 \frac{\partial}{\partial \theta},$$

$$\hat{b}(k, \omega, \theta) = 1 - \frac{\omega_{*e}}{\omega} + \frac{c_s^2}{\omega^2 q^2 R^2} \frac{\partial}{\partial \theta} P_2 \frac{\partial}{\partial \theta},$$

and

$$\begin{aligned} \hat{d}(k, \omega, \theta) = & \frac{\rho^2 v_A^2}{\omega^2 q^2 R^2} \frac{\partial}{\partial \theta} \nabla_1^2 \frac{\partial}{\partial \theta} - \left(1 - \frac{\omega_{*e}}{\omega}\right) \\ & + \left(1 - \frac{\omega_{*pe}}{\omega}\right) \frac{\omega_{De}(\theta)}{\omega} - \frac{c_s^2}{\omega^2 q^2 R^2} \frac{\partial}{\partial \theta} P_1 \frac{\partial}{\partial \theta}. \end{aligned}$$

The ion kinetic response functions, P and P_j ($j = 1, 2, 3$), are given by

$$P = \int d\mathbf{v} F_i(\mathbf{v}) \left(\frac{\omega - \omega_{*i}^T}{\omega - \omega_{Di}} \right) J_0^2 \left(\frac{k_1 v_1}{\omega_{ci}} \right), \quad (\text{A3})$$

$$P_j = \int d\mathbf{v} F_i(\mathbf{v}) \frac{\omega^{j-1} (\omega - \omega_{*i}^T)}{(\omega - \omega_{Di})^j} \frac{m_i v_{\parallel}^2}{T_i} J_0^2 \left(\frac{k_1 v_1}{\omega_{ci}} \right), \quad (\text{A4})$$

where $F_i(\mathbf{v}) = (2\pi v_i^2)^{-3/2} \exp(-v^2/2v_i^2)$ with $v_i = (T_i/m_i)^{1/2}$ and $\omega_{*i}^T = \omega_{*i} [1 + \eta_i (v^2/v_i^2 - 3/2)]$. The fluid limit of the P_j ($j = 1, 2, 3$) functions is

$$\begin{aligned} P_1^f = P_2^f = P_3^f \cong & (1 - \omega_{*i}/\omega) \Gamma_0(b) - (\omega_{*i}/\omega) \eta_i \{ \Gamma_0(b) \\ & + b [\Gamma_1(b) - \Gamma_0(b)] \}, \end{aligned} \quad (\text{A5})$$

with $\Gamma_j(b) = J_j(b) e^{-b}$ and $b = k_1^2 \rho_i^2 = k^2 \rho_i^2 (1 + s^2 \theta^2)$.

All frequencies are measured in units of c_s/r_n and the wave number k_θ in units of $\rho_s = c(m_i T_e)^{1/2}/eB$. The dimensionless complex frequency $\omega [c_s/r_n]$ is a function of the seven dimensionless parameters k , β_e , q , ϵ_n , s , η_i , and $\tau = T_e/T_i$. With the dimensionless variables, we write Eqs. (A1) and (A2) as

$$\begin{aligned} & (1 - \tau(P-1) + P_3^f \frac{\epsilon_n^2}{q^2 \omega^2} \frac{\partial^2}{\partial \theta^2}) \phi \\ & = \left(1 - \frac{\omega_{*e}}{\omega} + P_2^f \frac{\epsilon_n^2}{q^2 \omega^2} \frac{\partial^2}{\partial \theta^2}\right) \psi, \end{aligned} \quad (\text{A6})$$

$$\begin{aligned} & \left[\frac{\epsilon_n^2}{q^2 \omega^2} \frac{2}{\beta_e} \frac{\partial}{\partial \theta} k_1^2 \frac{\partial}{\partial \theta} + \left(1 - \frac{\omega_{*e}}{\omega}\right) \left(1 - \frac{\omega_{De}}{\omega}\right) \right. \\ & \left. + P_1^f \frac{\epsilon_n^2}{q^2 \omega^2} \frac{\partial^2}{\partial \theta^2} \right] \psi = \left(1 - \frac{\omega_{*e}}{\omega} + P_2^f \frac{\epsilon_n^2}{q^2 \omega^2} \frac{\partial^2}{\partial \theta^2}\right) \phi. \end{aligned} \quad (\text{A7})$$

1. Limiting regimes of the kinetic eigenmode equation

First we consider the limit that allows ion acoustic coupling terms to be zero with $\omega_A = (\epsilon_n/q)(2/\beta_e)^{1/2}$ fixed. If $q \rightarrow \infty$ but $q^2 \beta_e$ finite, Eqs. (A6) and (A7) reduce to the second-order differential equation

$$\begin{aligned} & [1 - \tau(P-1)] \left[\frac{\omega_A^2}{\omega^2} \frac{\partial}{\partial \theta} k_1^2 \frac{\partial}{\partial \theta} + \left(1 - \frac{\omega_{*e}}{\omega}\right) \right. \\ & \left. \times \left(1 - \frac{\omega_{De}}{\omega}\right) \right] \psi - \left(1 - \frac{\omega_{*e}}{\omega}\right)^2 \psi = 0, \end{aligned} \quad (\text{A8})$$

where we used

$$\frac{\psi}{\phi} = \frac{1 + \tau(1-P)}{1 - \omega_{*e}/\omega} \quad (\text{A9})$$

from Eq. (A6) and note that

$$E_{\parallel} = ik_{\parallel} \phi (1 - \psi/\phi).$$

The eigenmodes of Eq. (A8) have been analyzed in earlier works.^{21,23-25} With the full ion kinetic velocity space integral P , we give the results of the kinetic effects on MHD ballooning mode.

Equation (A8) also governs the toroidal η_i mode in the low-beta limit

$$\omega_A^2 \rightarrow \infty \quad \text{then} \quad D_{ES}(\omega, k) = 1 + \tau(1-P) = 0, \quad (\text{A10})$$

with the mode characteristics ($|\phi| \gg |\psi|$). In the high-beta limit, Eq. (A8) reduces to the MHD ballooning mode ($|\phi| \sim |\psi|$) for $k \rightarrow 0$ at finite ω .

In the $\beta \rightarrow 0$ limit, Eq. (A8) reduces to

$$[1 - \tau(P-1)] \frac{\omega_A^2}{\omega^2} \frac{\partial}{\partial \theta} k_1^2 \frac{\partial}{\partial \theta} \psi = 0. \quad (\text{A11})$$

If we assume $D_{ES} = [1 - \tau(P-1)] \neq 0$, then we obtain the solution of Eq. (A11) as $\psi \sim \tan^{-1} \theta$, which is an unphysical solution having $\int d\theta \psi^2 \rightarrow \infty$. Thus, to have a solution that tends to zero for large θ , we must have

$$D_{ES}(k, \omega, \theta = 0) = [1 - \tau(P-1)] = 0, \quad (\text{A12})$$

which is the local dispersion relation of toroidal η_i mode.

Dispersion relation Eq. (A12) gives unstable η_i mode when

$$\eta_i > \eta_c \sim \frac{2}{3} \quad \text{and} \quad \epsilon_{Ti} = r_{Ti}/R < 0.35. \quad (\text{A13})$$

Above the threshold, the mode has $\omega_k \simeq \omega_{Di} = -2k\epsilon_n$ and $\gamma_k \sim v_i/(Rr_{Ti})^{1/2}$. Recent H-mode discharge experiments show inverted gradient profiles with $\eta_i < 0$ and $\epsilon_n < 0$. For the dissipative drift wave and the trapped electron mode, the inverted profiles show substantial gain in stability for $\nu_{*e} < 0.3$ regime. For a fixed or local value of θ , the condition $\text{Im } P = 0$ yields the marginal stability frequency

$$\omega_m \cong \frac{1 + \frac{3}{2}|\eta_i|}{1 - |\eta_i|/|\epsilon_n|} \omega_{*i}$$

and

$$\text{Re } P(\omega_m) \cong |\eta_i/\epsilon_n| \Gamma_0(b),$$

which leads to the instability condition of

$$\epsilon_{Ti} < \frac{\tau \Gamma_0(b)}{1 + \tau} = \frac{\Gamma_0(b)}{1 + T_i/T_e} \leq \frac{1}{1 + T_i/T_e} \quad (\text{A14})$$

for $\epsilon_{Ti} = r_{Ti}/R = \epsilon_n/\eta_i$ from a Nyquist diagram.

2. Electrostatic toroidal integral equation

In the limit where magnetic shear determines the mode structure and the drift velocities are taken local in θ , the

velocity integrals can be done without the expansion in $P_{\parallel} \sim k_{\parallel}^2 v_i^2 / \omega^2$ defined in Eq. (12). We obtain the integral equation

$$(1 + \tau)\phi(k_x) = \int_{-\infty}^{+\infty} K(k_x, k'_x) \phi(k'_x) dk'_x, \quad (\text{A15})$$

where

$$K(k_x, k'_x) = \frac{2}{\sqrt{2\pi}} \int_{-\infty}^0 \frac{e^{-i\omega t} e^{-(k'_x - k_x)^2 / 4\sigma_t^2}}{(1 + a_t)\sqrt{a_t}} G(t) dt, \quad (\text{A16})$$

with the kinetic response function

$$G(T) = \frac{\omega_{*e}}{t\sqrt{2\sigma_t}} \left[\frac{\omega}{\omega_{*e}} \tau + 1 - \frac{3}{2} \eta_i + \frac{2\eta_i}{(1 + a_t)} \right] \times \left(1 - \frac{k_{\perp}^2 + k_{\perp}'^2}{2\tau(1 + a_t)} + \frac{k_{\perp} k_{\perp}'}{\tau(1 + a_t)} \frac{I_1}{I_0} \right) + \frac{\eta_i (k'_x - k_x)^2}{4a_t \sigma_t^2} \Gamma_0(k_{\perp}, k_{\perp}'), \quad (\text{A17})$$

where

$$a_t = 1 + i(2\epsilon_n \omega_{*e} t / \tau), \\ \sigma_t = (1/\tau a_t) (L_n / L_s)^2, \\ \Gamma_0(k_{\perp}, k_{\perp}') = I_0 [k_{\perp} k_{\perp}' / \tau(1 + a_t)] \times \exp[-k_{\perp}^2 + k_{\perp}'^2 / 2\tau(1 + a_t)], \\ k_{\perp}^2 = k_x^2 + k_y^2, \quad k_{\perp}'^2 = k_x'^2 + k_y'^2,$$

and $\tau = T_e / T_i$. For $s \rightarrow 0$, the matrix $K(k_x, k'_x)$ is diagonal and the eigenmodes are $\phi(k_x) = \delta(k_x - q)$ with the $q = 0$ mode from Eq. (A15) giving the local toroidal dispersion in Eq. (2). For $|\omega| \gg k_{\parallel} v_i, \omega_{Di}$, the small t limit $G(t) = G(0) + G'(0)t + \dots$ of Eq. (A16) returns the differential equation valid for $P_{\parallel} < 1$.

¹S. M. Wolfe and M. Greenwald, Nucl. Fusion **26**, 329 (1986).

²F. X. Söldner, E. R. Müller, F. Wagner, H. S. Bosch, A. Eberhagen, H. U. Fahrback, G. Fussmann, O. Gehre, K. Gentle, J. Gernhardt, O. Gruber, W. Herrmann, G. Janeschitz, M. Kornherr, K. Krieger, H. M. Mayer, K. McCormick, H. D. Murmann, J. Neuhauser, R. Nolte, W. Poschenrieder, H. Röhr, K.-H. Steuer, U. Stroth, N. Tsois, and H. Verbeek, Phys. Rev. Lett. **61**, 1105 (1988).

³S. D. Scott, P. H. Diamond, R. J. Fonck, R. J. Goldston, R. B. Howell, K. P. Jaehnig, G. Schilling, E. J. Synakowski, M. C. Zarnstorff, C. E. Bush, E. Fredrickson, K. W. Hill, A. C. Janos, D. K. Mansfield, D. K. Owens, H. Park, G. Pautasso, R. T. Ramsey, J. Schivell, G. D. Tait, W. M. Tang, and G. Taylor, Phys. Rev. Lett. **64**, 531 (1990).

⁴S. D. Scott, V. Arunasalam, C. W. Barnes, M. G. Bell, M. Bitter, R. Boivin, N. L. Bretz, R. Budny, C. E. Bush, A. Cavallo, T. K. Chu, S. A. Cohen, P. Colestock, S. L. Davis, D. L. Dimock, H. F. Dylla, P. C. Efthimion, A. B. Erhardt, R. J. Fonck, E. Fredrickson, H. P. Furth, R. J. Goldston, G. Greene, B. Grek, L. R. Grisham, G. Hammett, R. J. Hawryluk, H. W. Hendel, K. W. Hill, E. Hinnov, D. J. Hoffman, J. Hosea, R. B. Howell, H. Hsuan, R. A. Hilse, K. P. Jaehnig, A. C. Janos, D. Jassby, F. Jobs, D. W. Johnson, L. C. Johnson, R. Kaita, C. Kieras-Phillips, S. J. Kilpatrick, P. H. LaMarche, B. LeBlanc, R. Little, D. M. Manos, D. K. Mansfield, E. Mazzucato, M. P. McCarthy, D. C. McCune, K. McGuire, D. H. McNeill, D. M. Meade, S. S. Medley, D. R. Mikkelsen, R. Motley, D. Mueller, J. A. Murphy, Y. Nagayama, R. Nazakian, D. K. Owens, H. Park, A. T. Ramsey, M. H. Redi, A. L. Roquemore, P. H. Rutherford, G. Schilling, J. Schivell, G. L. Schmidt, J. Stevens, B. C. Stratton, W. Stodieck, E. J. Synakowski, W. M. Tang, G. Taylor, J. R. Timberlake, H. H. Towner, M. Ulrickson, S. von Goeler, R. Wieland, M. Williams, J. R. Wilson, K.-L. Wong, S. Yoshikawa, K. M. Young, M. C. Zarnstorff, and

S. J. Zweben, Phys. Fluids B **2**, 1300 (1990).

⁵M. C. Zarnstorff, C. W. Barnes, P. C. Efthimion, G. W. Hammett, W. Horton, R. A. Hulse, D. K. Mansfield, E. S. Marmor, K. McGuire, G. Rewoldt, B. C. Stratton, E. J. Synakowski, W. Tang, J. Terry, X. Q. Xu, M. G. Bell, M. Bitter, N. L. Bretz, R. Budny, C. E. Bush, G. J. Fonck, E. D. Fredrickson, H. P. Furth, R. J. Goldston, B. Grek, R. J. Hawryluk, K. W. Hill, H. Hsuan, D. W. Johnson, D. C. McCune, D. M. Meade, D. Mueller, D. K. Owens, H. K. Park, A. T. Ramsey, M. N. Rosenbluth, J. Schivell, G. L. Schmidt, S. D. Scott, G. Taylor, and R. M. Wieland, in *Plasma Physics and Controlled Nuclear Fusion Research, 1990*, Proceedings of the 12th International Conference, Washington (IAEA, Vienna, 1991), Vol. I, p. 109.

⁶M. C. Zarnstorff, N. L. Bretz, P. C. Efthimion, G. Hammett, W. Horton, R. Hulse, D. Mansfield, E. Marmor, K. McGuire, G. Rewoldt, B. Stratton, E. Synakowski, W. Tang, J. Terry, X. Xu, M. Bell, M. Bitter, N. Bretz, R. Budny, C. Bush, R. Fonck, E. Fredrickson, H. Furth, R. Goldston, B. Grek, R. Hawryluk, K. Hill, H. Hsuan, R. A. Hulse, D. Johnson, M. McCune, D. Meade, D. Mueller, D. Owens, H. Park, A. Ramsey, M. Rosenbluth, J. Schivell, G. Schmidt, S. Scott, G. Taylor, and R. Wieland, in *Proceedings of the 17th European Physical Society Conference on Controlled Fusion and Plasma Heating*, Amsterdam (European Physical Society, Budapest, 1990), Vol. I, p. 39.

⁷H. Biglari, P. H. Diamond, and M. N. Rosenbluth, Phys. Fluids B **1**, 109 (1989).

⁸S. Hamaguchi and W. Horton, Phys. Fluids B **2**, 1833, 3040 (1990).

⁹W. Horton, Phys. Rep. **192**, 177 (1990).

¹⁰G. W. Hammett and F. W. Perkins, Phys. Rev. Lett. **64**, 3019 (1990).

¹¹S. Hamaguchi and W. Horton, Plasma Phys. Controlled Fusion **34**, 203 (1992).

¹²M. Kotschenreuther, H. L. Berk, R. Denton, S. Hamaguchi, W. Horton, C.-B. Kim, M. Lebrun, P. Lyster, S. Mahajan, W. H. Miner, P. J. Morrison, D. W. Ross, R. D. Sydora, T. Tajima, J. B. Taylor, P. M. Valanju, H. V. Wong, S. Y. Xiao, and Y. Z. Yang, in *Plasma Physics and Controlled Nuclear Fusion Research, 1990*, Proceedings of the 13th International Conference, Washington (IAEA, Vienna, 1991), Vol. II, p. 361.

¹³J. Y. Kim and W. Horton, Phys. Fluids B **3**, 1167 (1991).

¹⁴R. R. Dominguez and R. E. Waltz, Phys. Fluids **31**, 3147 (1988).

¹⁵W. Horton, B. G. Hong, and W. M. Tang, Phys. Fluids **31**, 2971 (1988).

¹⁶F. Romanelli, Phys. Fluids B **1**, 1018 (1989).

¹⁷T. S. Hahm and W. M. Tang, Phys. Fluids B **1**, 1185 (1989).

¹⁸X. Q. Xu and M. N. Rosenbluth, Phys. Fluids B **3**, 627 (1991).

¹⁹S. C. Cowley, R. M. Kulsrud, and R. V. Sudan, Phys. Fluids B **3**, 2767 (1991).

²⁰R. R. Dominguez and M. N. Rosenbluth, Nucl. Fusion **29**, 844 (1989).

²¹B. G. Hong, W. Horton, and D. I. Choi, Plasma Phys. Controlled Fusion **31**, 1291 (1989); B. G. Hong, W. Horton, and D.-I. Choi, Phys. Fluids B **1**, 1589 (1989).

²²W. Horton, D. I. Choi, and W. M. Tang, Phys. Fluids **24**, 1077 (1981).

²³C. Z. Cheng, Nucl. Fusion **22**, 773 (1982).

²⁴W. M. Tang, G. Rewoldt, C. Z. Cheng, and M. S. Chance, Nucl. Fusion **25**, 151 (1985).

²⁵R. R. Dominguez and R. W. Moore, Nucl. Fusion **26**, 85 (1986).

²⁶J. Q. Dong, P. N. Guzdar, and Y. C. Lee, Phys. Fluids **30**, 2694 (1987).

²⁷H. Nordman, J. Weiland, and A. Jarmen, Nucl. Fusion **30**, 983 (1990).

²⁸A. Rogister, G. Hasselberg, F. Waelbroeck, and J. Weiland, Nucl. Fusion **28**, 1053 (1988).

²⁹J. Nilsson, M. Liljeström, and J. Weiland, Phys. Fluids B **2**, 2568 (1990).

³⁰G. Rewoldt and W. M. Tang, Phys. Fluids B **2**, 318 (1990); Bull. Am. Phys. Soc. **35**, 1981 (1990).

³¹R. Bravenec, D. W. Ross, P. M. Schoch, D. L. Brower, J. W. Heard, R. L. Hickok, P. W. Terry, A. J. Wootton, and X. Z. Yang, Nucl. Fusion **31**, 687 (1991).

³²M. Tang, Nucl. Fusion **18**, 1089 (1978).

³³W. Horton and R. D. Estes, Nucl. Fusion **19**, 203 (1979).

³⁴R. E. Waltz, Phys. Fluids **26**, 169 (1983).

³⁵D. E. Kim, D.-I. Choi, W. Horton, P. N. Yushmanov, and V. V. Parail, Phys. Fluids B **2**, 547 (1990).

³⁶S. Hamaguchi and W. Horton, Phys. Fluids B **4**, 319 (1992).

³⁷Y. B. Kim and P. H. Diamond, submitted to Phys. Fluids B.

³⁸T. Tajima, W. Horton, P. J. Morrison, J. Schutkeker, T. Kamimura, K. Mima, and Y. Abe, Phys. Fluids B **3**, 839 (1991).

³⁹M. B. Isichenko and W. Horton, Comments Plasma Phys. Controlled Fusion **14**, 249 (1991).

⁴⁰W. Horton, J. E. Sedlak, D. I. Choi, and B. G. Hong, Phys. Fluids **28**, 3050 (1985).